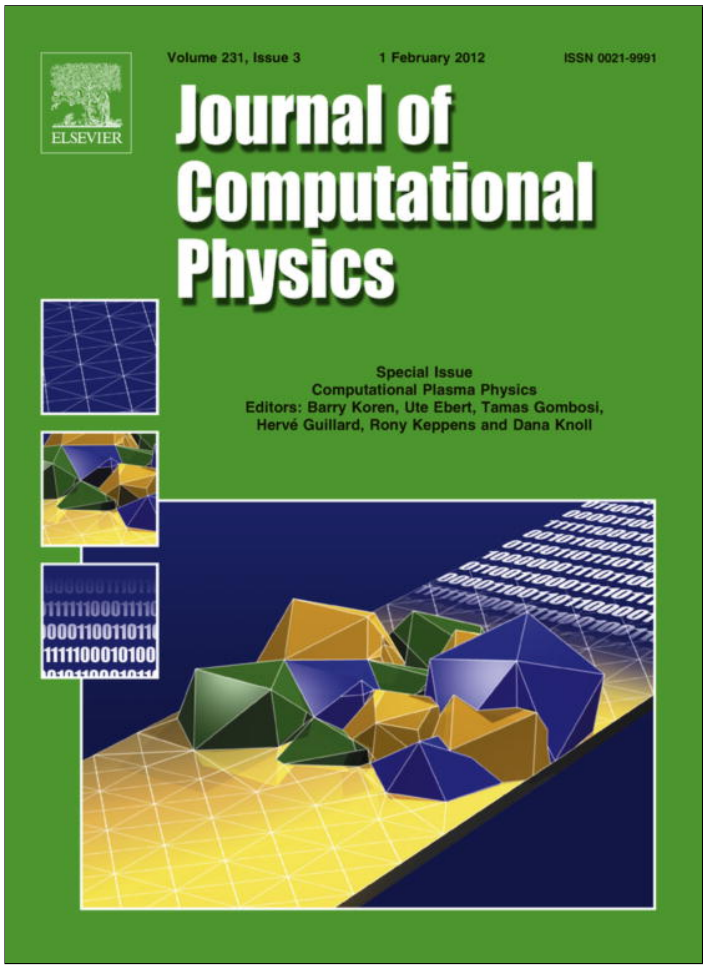

Journal of Computational Physics 231 (2012) 822–838

Contents lists available at ScienceDirect

Journal of Computational Physics

journal homepage: www.elsevier.com/locate/jcp

Review of implicit methods for the magnetohydrodynamic description of magnetically confined plasmas

S.C. Jardin

Princeton Plasma Physics Laboratory, Princeton, NJ 08543, USA

ARTICLE INFO

Article history:
Available online 25 December 2010

Keywords:
Magnetohydrodynamics
Implicit methods
Plasma physics
Fusion

ABSTRACT

Implicit algorithms are essential for predicting the slow growth and saturation of global instabilities in today's magnetically confined fusion plasma experiments. Present day algorithms for obtaining implicit solutions to the magnetohydrodynamic (MHD) equations for highly magnetized plasma have their roots in algorithms used in the 1960s and 1970s. However, today's computers and modern linear and non-linear solver techniques make practical much more comprehensive implicit algorithms than were previously possible. Combining these advanced implicit algorithms with highly accurate spatial representations of the vector fields describing the plasma flow and magnetic fields and with improved methods of calculating anisotropic thermal conduction now makes possible simulations of fusion experiments using realistic values of plasma parameters and actual configuration geometry. This article is a review of these developments.

1. Introduction

This article is a review of the progress made during the last 35 years in developing accurate and efficient implicit algorithms for simulating the global dynamics of strongly magnetized low-β (ratio of plasma to magnetic pressure) plasmas such as exist in modern magnetic fusion experiments; in particular the tokamak configuration [1]. Other, related confinement configurations that these methods are useful for include stellarators, reversed field pinches, spheromaks, and spherical tori. We limit our discussion to algorithms for solving the magnetohydrodynamic (MHD) equations [2], in which the plasma is described as a conducting fluid. Several forms of these equations are summarized in Appendix B. Efforts at extending this work to include intrinsically kinetic effects are presently underway, but this will not be covered in the present review.

The typical geometry of a tokamak experiment is shown in Fig. 1 where a cylindrical (R,φ,Z) coordinate system is used. The equilibrium magnetic field is axisymmetric; independent of the toroidal angle φ. The magnetic field is composed of a toroidal field, which is into the plane of the paper, and a poloidal field, which lies within the plane of the paper. The magnetic field lines interior to the separatrix surface form closed flux surfaces on which the temperature, pressure, and density are nearly constant. These are shown as solid curves in the figure. The ratio of the number of times a magnetic field line goes the long way around the torus to the number of times it goes the short way around on one of these surfaces is called the safety factor, which we denote as q. It typically varies from 1 near the magnetic axis to 3 or 4 near the edge. Exterior to the separatrix surface, the magnetic surfaces are open and the field lines intersect the vacuum vessel or other structures. The plasma on these open surfaces will necessarily be very low pressure, density, and temperature. The vacuum vessel is sometimes modeled as a perfect conductor, but in reality has some electrical resistance, which can be important for some plasma dynamics [3,4]. Exterior to the vacuum vessel, it is normally assumed that a vacuum exists so that the free-space

E-mail address: jardin@pppl.gov

0021-9991/$ - see front matter © 2010 Elsevier Inc. All rights reserved.
doi:10.1016/j.jcp.2010.12.025

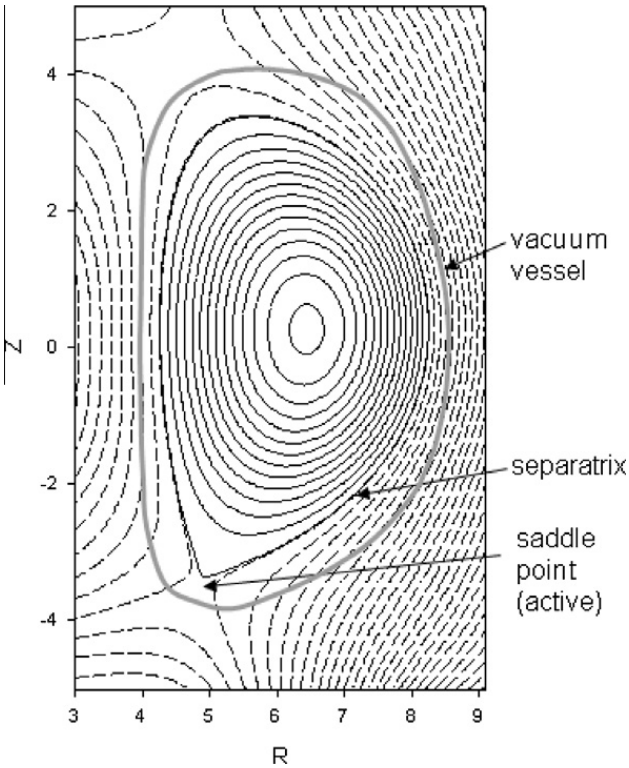

Fig. 1. In a tokamak, the equilibrium plasma is axisymmetric. Magnetic flux surfaces are closed interior to the separatrix and open exterior to it. Plasma is surrounded by a metallic vacuum vessel.

Maxwell equations are satisfied. This is the geometry we are interested in simulating, although much of the algorithm development leading up to simulations in this geometry has occurred using much simpler geometry.

In Section 2 we review the reasons for the multiple timescales that exist when describing the global dynamics of magnetized plasma, and hence the need for an implicit algorithm. Section 3 traces back the origins of modern algorithms for treating the hyperbolic terms (ideal MHD) to similar methods proposed for implicit hydrodynamics in the 1960s. In Section 4 we discuss some of the considerations in choosing a spatial representation, including the choice of variables used in representing the vector fields. We discuss implicit treatment of the anisotropic heat conduction in Section 5, and techniques for dealing with the terms that occur in the two-fluid (2F) description in Section 6. Section 7 contains a short summary and some observations. In Appendix A, we show the relation of the algorithms most widely used for implicit treatment of the hyperbolic terms to the Schur complement of a matrix.

2. The need for an implicit algorithm

Global plasma instabilities are termed either "ideal" or "resistive" depending on the minimum equation set that is required to describe their onset. Ideal instabilities require only the ideal MHD equations [5], while resistive instabilities require the presence of resistivity, or other forms of dissipation. In general, resistive instabilities occur on significantly slower timescales than do ideal instabilities since the resistivity in high temperature plasma is very low.

There is a wide separation in timescales even within phenomena described by the ideal MHD equations in tokamak geometry. There are three characteristic wave propagation velocities in ideal MHD: that of the slow wave V_S, the Alfvén wave V_A, and the fast wave V_F. These satisfy $V_S \ll V_A < V_F$. Since the fast wave is the only one that compresses the magnetic field, a motion that is highly stabilizing, all low-β tokamak ideal MHD instabilities are associated with the slow wave and the Alfvén wave. The plasma will "slip through" the background field rather than compress it. However it is the fast wave that sets the maximum allowable time step when using an explicit time advance.

To better understand the time step restriction imposed by the presence of the fast wave, consider the timescales associated with the three types of waves. The slow wave and Alfvén wave only propagate in the direction parallel to the background magnetic field whereas the fast wave's propagation is nearly isotropic [2]. If we denote the local safety factor as q and the local aspect ratio as ε, then the ratio of the transit times of these three waves is: $q\varepsilon^{-2}$: $q\varepsilon^{-1}$: 1. However, the difference in the explicit time step constraint associated with the three waves is much more extreme than this. The spatial resolution requirements perpendicular to the magnetic field are much more severe than those parallel to the magnetic field, making the Courant–Friedrichs–Lewy (CFL) [6] condition associated with the fast wave much more restrictive than that

associated with the others; typically by two or more orders of magnitude. An implicit treatment of at least the fast wave is therefore essential if one is to follow even relatively rapid growing ideal MHD instabilities.

Resistive instabilities present even more of a timescale problem. The Lundquist number, S, is the ratio of the resistive diffusion time for the magnetic field to the Alfvén wave transit time. If we denote the minor radius as a, the poloidal magnetic field as B_P, the plasma resistivity as η, the number density as n, the ion mass as M_i, and the permeability of free space as $\mu_0 = 4\pi \times 10^{-7}$, then we can approximate this as (SI units):

$$S = \sqrt{\frac{\mu_0}{nM_i}}\frac{aB_p}{\eta}. \tag{1}$$

In modern fusion experiments, this number is typically in the range: $S \sim 10^6 - 10^9$. Resistive instabilities will grow on times proportional to inverse fractional powers of this multiplied by the Alfvén wave transit time: $\tau_{RI} \sim S^{-\alpha}\tau_A$ where typically $\alpha \sim 1/3 - 3/5$ [7,8]. The initial growth of these instabilities involves plasma motion highly localized in the vicinity of a particular flux surface, necessitating very high spatial resolution in the direction perpendicular to the magnetic field. During the nonlinear growth, it is typical to have $\alpha \sim 1$[9] so that very long integration time scales are required. It is clear that a highly implicit treatment of the ideal MHD wave terms (hyperbolic terms) is essential if one is interested in simulating these slowly growing resistive instabilities.

3. Implicit algorithms for time advancing the hyperbolic terms

If the (small) resistive and other dissipative terms are neglected, the resistive MHD equations reduce to the ideal MHD equations, a symmetric hyperbolic system of equations. In this section, we review progress in developing implicit algorithms for this type of system of equations.

3.1. Implicit hydrodynamics

The algorithm now widely used to obtain implicit solutions (and hence enable large time steps) for the MHD equations has its roots in the ICE algorithm of Harlow and Amsden for hydrodynamics [10]. The essence of this algorithm can be illustrated by applying it to the 2D isothermal hydrodynamic system of equations:

$$\frac{\partial\rho}{\partial t} + \frac{\partial m_x}{\partial x} + \frac{\partial m_y}{\partial y} = 0, \tag{2a}$$

$$\frac{\partial m_x}{\partial t} + \frac{\partial}{\partial x}(\rho u^2) + \frac{\partial}{\partial y}(\rho u v) + c^2\frac{\partial\rho}{\partial x} = 0, \tag{2b}$$

$$\frac{\partial m_y}{\partial t} + \frac{\partial}{\partial x}(\rho u v) + \frac{\partial}{\partial y}(\rho v^2) + c^2\frac{\partial\rho}{\partial y} = 0. \tag{2c}$$

Here ρ is the fluid density, $m_x \equiv \rho u$ and $m_y \equiv \rho v$ are momentum densities, and c^2 is a constant. The method is motivated by the need to treat the sound wave characteristics implicitly when the flow Mach number is small. This is accomplished by using the advanced time value of the momentum density in the density evolution equation, Eq. (2a), and the advanced time value of the density in the momentum density evolution equations, Eqs. (2b), (2c). Introduce the time step δt and consider the time advance from time n (denoted with a superscript) to time $n+1$. Using "dots" to denote time differentiation; i.e. $\dot{a} \equiv \partial a/\partial t = (a^{n+1} - a^n)/\delta t$ for any scalar quantity a, we can introduce an implicit parameter θ and write the implicit time advance equations as

$$\dot{\rho} + \frac{\partial}{\partial x}(m_x^n + \theta\delta t\dot{m}_x) + \frac{\partial}{\partial y}(m_y^n + \theta\delta t\dot{m}_y) = 0, \tag{3a}$$

$$\dot{m}_x + \frac{\partial}{\partial x}\left[(\rho^n + \theta\delta t\dot{\rho})u^2\right] + \frac{\partial}{\partial y}[(\rho^n + \theta\delta t\dot{\rho})uv] + c^2\frac{\partial}{\partial x}(\rho^n + \theta\delta t\dot{\rho}) = 0, \tag{3b}$$

$$\dot{m}_y + \frac{\partial}{\partial x}[(\rho^n + \theta\delta t\dot{\rho})uv] + \frac{\partial}{\partial y}\left[(\rho^n + \theta\delta t\dot{\rho})v^2\right] + c^2\frac{\partial}{\partial y}(\rho^n + \theta\delta t\dot{\rho}) = 0. \tag{3c}$$

Those variables without a superscript or dot are evaluated at time level n. We can now use Eqs. (3b) and (3c) to eliminate $\dot{m}_x$ and $\dot{m}_y$ from Eq. (3a) to obtain

$$\begin{aligned}\dot{\rho} - (\theta\delta t)^2\left(\frac{\partial^2}{\partial x^2}\left[(u^2+c^2)\dot{\rho}\right] + 2\frac{\partial^2}{\partial y\partial x}[uv\dot{\rho}] + \frac{\partial^2}{\partial y^2}\left[(v^2+c^2)\dot{\rho}\right]\right)\\ = -\frac{\partial}{\partial x}(m_x^n) - \frac{\partial}{\partial y}(m_y^n) + \theta\delta t\left(\frac{\partial^2}{\partial x^2}\left[(u^2+c^2)\rho\right] + 2\frac{\partial^2}{\partial y\partial x}[uv\rho] + \frac{\partial^2}{\partial y^2}\left[(v^2+c^2)\rho\right]\right).\end{aligned} \tag{4}$$

Letting $\delta t\dot{\rho} = \rho^{n+1} - \rho^n$, and multiplying through by δt, we have

$$\rho^{n+1} - \rho^n - (\theta\delta t)^2\left(\frac{\partial^2}{\partial x^2}\left[(u^2+c^2)\rho^{n+1}\right] + 2\frac{\partial^2}{\partial y\partial x}[uv\rho^{n+1}] + \frac{\partial^2}{\partial y^2}\left[(v^2+c^2)\rho^{n+1}\right]\right)$$
$$= -\delta t\frac{\partial}{\partial x}(m_x^n) - \frac{\partial}{\partial y}\delta t(m_y^n) + \theta(1-\theta)(\delta t)^2\left(\frac{\partial^2}{\partial x^2}\left[(u^2+c^2)\rho\right] + 2\frac{\partial^2}{\partial y\partial x}[uv\rho] + \frac{\partial^2}{\partial y^2}\left[(v^2+c^2)\rho\right]\right). \tag{5}$$

This can be put into the form used in [10] by setting $\theta = 1$ (backward in time), using centered finite difference operators, and subtracting Eq. (3a) in the form

$$-\rho^n + \rho^{n-1} = \delta t\frac{\partial}{\partial x}(m_x^n) + \delta t\frac{\partial}{\partial y}(m_y^n). \tag{6}$$

This yields the finite difference equation for the new time density:

$$\rho_{i,j}^{n+1} - 2\rho_{i,j}^n + \rho_{i,j}^{n-1} - \frac{\delta t^2}{\delta x^2}\left[\left((u^2)_{i+1,j}^n + c^2\right)\rho_{i+1,j}^{n+1} - 2\left((u^2)_{i,j}^n + c^2\right)\rho_{i,j}^{n+1} + \left((u^2)_{i-1,j}^n + c^2\right)\rho_{i-1,j}^{n+1}\right]$$
$$-\frac{\delta t^2}{\delta y^2}\left[\left((v^2)_{i,j+1}^n + c^2\right)\rho_{i,j+1}^{n+1} - 2\left((v^2)_{i,j}^n + c^2\right)\rho_{i,j}^{n+1} + \left((v^2)_{i,j-1}^n + c^2\right)\rho_{i,j-1}^{n+1}\right]$$
$$-2\frac{\delta t^2}{\delta x\delta y}\begin{bmatrix}(uv)_{i+1/2,j+1/2}^n\rho_{i+1/2,j+1/2}^{n+1} - (uv)_{i+1/2,j-1/2}^n\rho_{i+1/2,j-1/2}^{n+1}\\ -(uv)_{i-1/2,j+1/2}^n\rho_{i-1/2,j+1/2}^{n+1} + (uv)_{i-1/2,j-1/2}^n\rho_{i-1/2,j-1/2}^{n+1}\end{bmatrix} = 0. \tag{7}$$

Subscripts denote the spatial index on an equally spaced Cartesian grid with $x = i\delta x$ and $y = j\delta y$. Eq. (7) is then solved iteratively for the new time density: $\rho_{i,j}^{n+1}$. Once this is obtained, it is used in the finite difference forms of Eqs. (3b) and (3c) to advance the momentum density from time n to $n + 1$. Eq. (7) is seen to be a diagonally dominant matrix equation that is readily solved by relaxation techniques. The noteworthy features of this unconditionally stable method are that (1) the matrix equation that needs to be solved is for only one variable, ρ^{n+1}, as the momentum variables at the new time level have been eliminated algebraically, and (2) the matrix equation is diagonally dominant and nearly symmetric, and thus well conditioned.

3.2. Implicit treatment of the fast wave

Consider now the ideal MHD equations (given in Appendix B), a purely hyperbolic system of equations. These are similar to the hydrodynamic equations, but are considerably more complicated in that they have additional characteristics. As discussed above, in a low-β strongly magnetized fusion plasma, such as a tokamak, the ideal MHD equations contain three types of wave solutions that differ greatly in their structure and propagation properties. Since the CFL condition for the fastest of these waves is unduly restrictive, some type of implicit treatment is required if one is to integrate the equations over times of interest. We can use the fact that the fast wave is the only one that compresses the magnetic field and hence has a non-zero divergence perpendicular to the field, $\nabla\cdot\mathbf{V}_\perp \neq 0$, [2] to isolate it for an implicit advance in a relatively simple equation. Consider the ideal MHD equations in the form:

$$\dot{\mathbf{V}} + \mathbf{V}\cdot\nabla\mathbf{V} + \frac{1}{\rho}\nabla\left(p + \frac{1}{2\mu_0}B^2\right) = +\frac{1}{\rho\mu_0}\mathbf{B}\cdot\nabla\mathbf{B}, \tag{8a}$$
$$\dot{p} + \mathbf{V}\cdot\nabla p + \gamma p\nabla\cdot\mathbf{V} = 0, \tag{8b}$$
$$\dot{\mathbf{B}} + \mathbf{V}\cdot\nabla\mathbf{B} + \mathbf{B}\nabla\cdot\mathbf{V}_\perp - \mathbf{B}\cdot\nabla\mathbf{V}_\perp = 0. \tag{8c}$$

Next, define the total (fluid + magnetic pressure) $P \equiv p + \frac{1}{2\mu_0}B^2$ and the perpendicular divergence of the velocity $\Delta \equiv \nabla_\perp\cdot\mathbf{V}$. By taking the perpendicular divergence of Eq. (8a) and adding Eq. (8b) to the inner product of $\mathbf{B}$ with Eq. (8c) we obtain [11]

$$\dot{P} + \left(\frac{1}{\mu_0}B^2 + \gamma p\right)\Delta + N = 0, \tag{9a}$$
$$\dot{\Delta} + \nabla_\perp\cdot\frac{1}{\rho}\nabla P + Q = 0. \tag{9b}$$

Here, we have defined

$$N \equiv \mathbf{V}\cdot\nabla p + \gamma p\nabla\cdot\mathbf{V}_\parallel + \frac{1}{\mu_0}\mathbf{B}\cdot\mathbf{V}\cdot\nabla\mathbf{B} - \frac{1}{\mu_0}\mathbf{B}\cdot\mathbf{B}\cdot\nabla\mathbf{V}_\perp, \tag{10a}$$
$$Q \equiv \nabla_\perp\cdot\left[\frac{-1}{\mu_0\rho}\mathbf{B}\cdot\nabla\mathbf{B} + \mathbf{V}\cdot\nabla\mathbf{V}\right]. \tag{10b}$$

In a manner analogous to what was done in going from Eq. (2) to Eq. (3), we construct a partially implicit time advance by evaluating the perpendicular velocity divergence and the total pressure in Eq. (9) at the advanced time to obtain

$$\dot{P} + \left(\frac{1}{\mu_0}B^2 + \gamma p\right)\left(\Delta^n + \theta\delta t\dot{\Delta}\right) + N = 0, \tag{11a}$$

$$\dot{\Delta} + \nabla_\perp \cdot \frac{1}{\rho}\nabla\left(P^n + \theta\delta t\dot{P}\right) + Q = 0. \tag{11b}$$

Next, use Eq. (11b) to eliminate $\dot{\Delta}$ from Eq. (11a) to obtain the single equation for the advanced time pressure:

$$P^{n+1} - (\theta\delta t)^2 c^2 \nabla_\perp \cdot \frac{1}{\rho}\nabla P^{n+1} = P^n + \delta t\left[-c^2\Delta^n - N + c^2\theta\delta t Q\right] + \theta(1-\theta)\delta t^2 c^2 \nabla_\perp \cdot \frac{1}{\rho}\nabla P^n. \tag{12}$$

Here, we have defined $c^2 \equiv \frac{1}{\mu_0}B^2 + \gamma p$. Again, we note that after applying centered spatial finite differencing operators, Eq. (12) becomes a well conditioned, diagonally dominant nearly symmetric matrix equation for the new time total pressure, very similar to the equation for the new time density in Eq. (7). The total pressure, P^{n+1}, can be readily solved for using relaxation or other techniques [11]. Once this is obtained, we can use it in Eq. (8a) to advance the velocity, and then use the advanced velocity in Eq. (8b) and (8c) to advance the pressure and magnetic field. The time step using this method need only obey the CFL condition for the Alfvén wave and slow wave, not the fast wave.

This basic technique of solving a separate equation for the advanced time total pressure has been extended to three dimensions in [12] and to 3D toroidal geometry [14]. However, in [12], the operator in Eq. (12) is replaced in their Eq. (32) by:

$$P^{n+1} - (\theta\delta t)^2\left[\gamma p^* \nabla_\perp \cdot \frac{1}{\rho}\nabla P^{n+1} - \mathbf{B}^* \cdot \nabla \times \frac{1}{\rho}\nabla P^{n+1} \times \mathbf{B}^*\right] = \cdots. \tag{13}$$

Here starred quantities are predicted values in their predictor–corrector algorithm. Eq. (13) is what results if all the terms in Eq. (8c) are retained in the implicit solve rather than just the one involving compression. It is not clear what the advantage of this is, or if the authors studied its effect. This algorithm was first successfully implemented in circular cylindrical geometry where the two equilibrium ignorable periodic coordinates were treated using a Fourier series expansion. In order to obtain separable equations to facilitate rapid inversion, the quantities p and $\mathbf{B}^*$ were approximated as being independent of the angles during the matrix solve [12]. This was later extended to toroidal geometry [13].

3.3. Semi-implicit treatment of the fast wave

At about the same time as [12] appeared; Harned and Kerner [15] developed a semi-implicit algorithm that also allows exceeding the CFL condition for the fast wave. Although not cited in this first paper, a similar semi-implicit algorithm had been used previously by others in large scale meteorological calculations to eliminate the severe time step constraint due to external gravity waves. This technique was shown to be exceptionally efficient when using a spectral representation [16] but had also been shown to be effective when using a finite difference model [17]. This early meteorological work is reviewed in [18] and referred to in later MHD publications[19].

The Harned and Kerner algorithm is noteworthy in several respects: (1) it solves for the velocity field (rather than the total pressure) with an implicit operator. This is important in that it was essential for subsequent extensions of this technique to an implicit treatment of the other ideal MHD characteristics, (2) it uses an approximate implicit operator rather than the full operator. This has the potential for greatly increasing the efficiency of the method for a nonlinear problem since the same (approximate) implicit operator could be used repeatedly without having to be inverted each time step, and (3) the same operator appears on each side of the equals sign in the equation for the new time velocity; it operates on $\mathbf{V}^{n+1}$ on the left and $\mathbf{V}^n$ on the right. This provides a convenient prescription for developing a second order in time implicit operator that again allowed for generalization in future works.

To derive the Harned and Kerner algorithm, consider the ideal MHD equations as given in Eq. (8). Analogous to Eq. (11), we evaluate only the terms that contribute to the fast wave at the advanced time:

$$\dot{\mathbf{V}} + \mathbf{V}\cdot\nabla\mathbf{V} + \frac{1}{\rho}\nabla\left[p + \theta\delta t\dot{p} + \frac{1}{2\mu_0}B^2 + \frac{1}{\mu_0}\theta\delta t\mathbf{B}\cdot\dot{\mathbf{B}}\right] = +\frac{1}{\rho\mu_0}\mathbf{B}\cdot\nabla\mathbf{B}, \tag{14a}$$

$$\dot{p} + \mathbf{V}\cdot\nabla p + \gamma p\nabla\cdot(\mathbf{V} + \theta\delta t\dot{\mathbf{V}}) = 0, \tag{14b}$$

$$\dot{\mathbf{B}} + \mathbf{V}\cdot\nabla\mathbf{B} + \mathbf{B}\nabla\cdot(\mathbf{V} + \theta\delta t\dot{\mathbf{V}}) - \mathbf{B}\cdot\nabla\mathbf{V} = 0. \tag{14c}$$

Substitution of Eq. (14b) and (14c) to eliminate $\dot{p}$ and $\dot{\mathbf{B}}$ from Eq. (14a), and *keeping only those terms in* Eq. (14b) and (14c) *which multiply* $\dot{\mathbf{V}}$ yields

$$\dot{\mathbf{V}} - (\theta\delta t)^2\frac{1}{\rho}\nabla\left[(\gamma p + \mathbf{B}^2)\nabla\cdot\dot{\mathbf{V}}\right] = -\mathbf{V}\cdot\nabla\mathbf{V} - \frac{1}{\rho}\nabla\left[p + \frac{1}{2\mu_0}B^2\right] + \frac{1}{\rho\mu_0}\mathbf{B}\cdot\nabla\mathbf{B}. \tag{15a}$$

The semi-implicit method now introduces a constant, A_0^2, and replaces Eq. (15a) with the following modified form:

$$\dot{\mathbf{V}} - (\delta t)^2 A_0^2\nabla\nabla\cdot\dot{\mathbf{V}} = -\mathbf{V}\cdot\nabla\mathbf{V} - \frac{1}{\rho}\nabla\left[p + \frac{1}{2\mu_0}B^2\right] + \frac{1}{\rho\mu_0}\mathbf{B}\cdot\nabla\mathbf{B}. \tag{15b}$$

The discrete version of Eq. (15b) is obtained by substituting $\dot{\mathbf{V}} = (\mathbf{V}^{n+1} - \mathbf{V}^n)/\delta t$ and applying central finite differences and/or a Fourier series expansion. This, together with the discrete forms of Eqs. (14b) and (14c) with $\theta \geqslant 1/2$, is shown to be numerically stable for time steps that exceed the CFL condition for the fast wave (but not the Alfven wave) as long as $A_0^2 \geqslant (1/4\rho_0)(\gamma p_0 + \mathbf{B}_0^2)\cdot$ This was implemented in a predictor–corrector algorithm in which the explicit forms (with $\theta = 0$) of Eq. (14) were used to calculate predicted values of $\mathbf{V}$, $\mathbf{B}$, and p. Then, the velocity at the new time level, $\mathbf{V}^{n+1}$, was calculated from Eq. (15b). This and the predicted values of $\mathbf{B}$ and p were then used in Eqs. (14b) and (14c) to get new time values of these quantities.

3.4. Semi-implicit treatment of the alfven and fast waves

Not long after the semi-implicit operator for the fast wave in Eq. (15b) was derived, it was extended by Harned and Schnack [19] to include the Alfven wave. Consider the full ideal MHD equations applied to a uniform magnetic field configuration, but with all the terms that lead to wave solutions evaluated at the advanced time. The analogue of Eq. (14) is

$$\dot{\mathbf{V}} + \mathbf{V}\cdot\nabla\mathbf{V} + \frac{1}{\rho}\nabla(p + \theta\delta t\dot{p}) = +\frac{1}{\rho\mu_0}\left[\nabla\times(\mathbf{B} + \theta\delta t\dot{\mathbf{B}})\right]\times\mathbf{B}, \tag{16a}$$

$$\dot{p} + \mathbf{V}\cdot\nabla p + \gamma p\nabla\cdot(\mathbf{V} + \theta\delta t\dot{\mathbf{V}}) = 0, \tag{16b}$$

$$\dot{\mathbf{B}} = \nabla\times\left[(\mathbf{V} + \theta\delta t\dot{\mathbf{V}})\times\mathbf{B}\right]. \tag{16c}$$

Using Eqs. (16b) and (16c) to eliminate $\dot{p}$ and $\dot{\mathbf{B}}$ from Eq. (16a), and keeping only the terms in the substitution proportional to $\dot{\mathbf{V}}$ gives the following operator equation for the time derivative of the velocity:

$$\dot{\mathbf{V}} - (\theta\delta t)^2\frac{1}{\rho}\nabla\left(\gamma p\nabla\cdot\dot{\mathbf{V}}\right) - \frac{1}{\rho\mu_0}(\theta\delta t)^2\left[\nabla\times\left(\nabla\times[\dot{\mathbf{V}}\times\mathbf{B}]\right)\right]\times\mathbf{B} = -\mathbf{V}\cdot\nabla\mathbf{V} - \frac{1}{\rho}\nabla p + \frac{1}{\rho\mu_0}[\nabla\times\mathbf{B}]\times\mathbf{B}. \tag{17a}$$

The semi-implicit operator used in [19] replaced the magnetic field on the left in Eq. (17) by a vector quantity with constant coefficients: $C_0 = C_x\hat{x} + C_y\hat{y} + C_z\hat{z}$. The pressure term is dropped, with the reasoning that it does not enter into the Alfvén wave and enters into the fast wave with the same form as the perpendicular magnetic field. Therefore, the semi-implicit approximation to Eq. (17a) is just

$$\dot{\mathbf{V}} - \frac{1}{\rho_0\mu_0}\delta t^2\left[\nabla\times\left(\nabla\times\left[\dot{\mathbf{V}}\times\mathbf{C_0}\right]\right)\right]\times\mathbf{C_0} = -\mathbf{V}\cdot\nabla\mathbf{V} - \frac{1}{\rho}\nabla p + \frac{1}{\rho\mu_0}[\nabla\times\mathbf{B}]\times\mathbf{B}. \tag{17b}$$

This was implemented in Cartesian geometry in [19] in the following way: first the velocity and field quantities are updated explicitly to a provisional time value $(*)$ in a predictor step by using Eq. (16) with $\theta = 0$. These provisional values are used to advance the velocity from time n to $n + 1$ using the semi-implicit Eq. (17b). They then use an average of the velocity at from time n and $n + 1$ and the field quantities at time value $(*)$ to perform a corrector step to advance the field variables from time n to $n + 1$. However, for the magnetic field (or vector potential), they then perform a final split semi-implicit advance where the resistive part of the MHD equations is included.

It is shown in [19] that this algorithm is unconditionally stable as long as $C_i \geqslant B_i$ everywhere for $i = x, y, z$ *with the crucial modification that all terms that appear in the semi-implicit operator as products as* C_iC_j *be replaced by* $C_i\,C_j\delta_{ij}$, *where* δ_{ij} *is the Kronecker delta.*

This work was extended in [20] to cylindrical geometry where a spectral representation was used in the periodic poloidal and axial coordinates. Define the semi-implicit operator in Eq. (17b) as

$$\mathbf{G}\{\dot{\mathbf{V}}\} \equiv \left[\nabla\times\left(\nabla\times\left[\dot{\mathbf{V}}\times\mathbf{C_0}\right]\right)\right]\times\mathbf{C_0}, \tag{18a}$$

Besides retaining only terms proportional to C_α^2, where now $\alpha = r,\theta,z$, they further ignored any coupling between V_Z and (V_r,V_θ), allowing the algorithm to retain a 2×2 block tridiagonal structure. An additional approximation that was considered in [20] was to approximate Eq. (18a) by the much simpler isotropic operator

$$\mathbf{G}\{\dot{\mathbf{V}}\} = C_0^2\nabla^2\dot{\mathbf{V}}. \tag{18b}$$

They present comparisons of long time simulations using Eqs. (18a) and Eqs. (18b) and conclude that the accuracy of the linear modes for a given time-step size is improved by using Eq. (18a) (including the modifications discussed above), but that far into the nonlinear phase of a reversed field pinch simulation the results of using the two approximate operators are similar.

It is also noteworthy in [20] that the leap-frog method was combined with the semi-implicit method in a way that reduced the dissipation of the algorithm. They define the field quantities at times offset from the velocity by half a time step. After performing a predictor–corrector step just for the field quantities which includes an implicit treatment of the resistive term, and a predictor step for the velocity that includes only the convective derivative term, they use these on the right side to Eq. (17b) to advance the velocity to the new time level.

The algorithm presented in [20] was later found to be unstable if significant plasma flow was present. However, it was shown that if the semi-implicit operator was included in both the predictor and corrector steps for the velocity, a method that was stable for CFL numbers based on the flow speed up to 1 could be obtained [21]. This was also demonstrated in [22].

3.5. The method of differential approximation

Consider now the ideal MHD equations where all the terms containing the pressure and magnetic field in the momentum equation are evaluated at the advanced time, as are all the terms containing the velocity in the pressure and magnetic field equations. The analogue of (14) and (16) is

$$\dot{\mathbf{V}} + \mathbf{V}\cdot\nabla\mathbf{V} + \frac{1}{\rho}\nabla(p + \theta\delta t\dot{p}) = +\frac{1}{\rho\mu_0}\left[\nabla\times(\mathbf{B} + \theta\delta t\dot{\mathbf{B}})\right]\times(\mathbf{B} + \theta\delta t\dot{\mathbf{B}}), \tag{19a}$$

$$\dot{p} + (\mathbf{V} + \theta\delta t\dot{\mathbf{V}})\cdot\nabla p + \gamma p\nabla\cdot(\mathbf{V} + \theta\delta t\dot{\mathbf{V}}) = 0, \tag{19b}$$

$$\dot{\mathbf{B}} = \nabla\times\left[(\mathbf{V} + \theta\delta t\dot{\mathbf{V}})\times\mathbf{B}\right]. \tag{19c}$$

In a manner closely analogous to the above, we linearized Eq. (19a) in the terms involving δt, and then use Eqs. (19b) and (19c) to eliminate $\dot{p}$ and $\dot{\mathbf{B}}$ from the linearized Eq. (19a). This yields

$$\dot{\mathbf{V}} - \frac{1}{\rho}(\theta\delta t)^2\mathbf{G}\{\dot{\mathbf{V}}\} = \frac{1}{\rho}(\theta\delta t)\mathbf{G}\{\mathbf{V}\} - \mathbf{V}\cdot\nabla\mathbf{V} - \frac{1}{\rho}\nabla p + \frac{1}{\rho\mu_0}(\nabla\times\mathbf{B})\times\mathbf{B}. \tag{20a}$$

Here, $\mathbf{G}$ is the full ideal MHD operator [23]

$$\mathbf{G}\{\dot{\mathbf{V}}\} = \nabla\times\left[\nabla\times(\dot{\mathbf{V}}\times\mathbf{B})\right]\times\mathbf{B} + (\nabla\times\mathbf{B})\times\left[\nabla\times(\dot{\mathbf{V}}\times\mathbf{B})\right] + \nabla\left[\dot{\mathbf{V}}\cdot\nabla p + \gamma p\nabla\cdot\dot{\mathbf{V}}\right]. \tag{20b}$$

Caramana [24] noted that it is the numerical dispersion coming from the implicit operator acting on $\dot{\mathbf{V}}$, i.e. the second term on the left in Eq. (20a), that is the primary numerical stabilization mechanism, rather than the first term on the right, that provides numerical dissipation. Thus, implicit methods can get rid of numerical dissipation by dropping that term and combining with leap-frog for the field advance equations (or by setting $\theta = 1/2$ in a θ-implicit scheme) and still have numerical stability with an arbitrarily large time step. He therefore replaced Eq. (20a) with [24]

$$\dot{\mathbf{V}} - \frac{1}{\rho}(\theta\delta t)^2\mathbf{G}\{\dot{\mathbf{V}}\} = -\mathbf{V}\cdot\nabla\mathbf{V} - \frac{1}{\rho}\nabla p + \frac{1}{\rho\mu_0}(\nabla\times\mathbf{B})\times\mathbf{B}. \tag{20c}$$

The system given by Eqs. (20c), (20b), (19b) and (19c) looks very similar to the semi-implicit method, Eq. (17b), but it has one important advantage. Since no additional approximations to the operator $\mathbf{G}$ were made, the eigenvalues of $\mathbf{G}$ are the same as the eigenvalues of the ideal MHD equations. This means that there is no mixing of the linear eigenvalues and thus the system given by Eqs. (20b), (20c), (19b) and (19c) can be used to faithfully compute eigenvectors of the original system. In particular, there is no intrinsic "spectral pollution" [25] introduced in this algorithm whereby eigenmodes associated with the fast waves will produce artificial stabilization of the possibly unstable eigenmodes associated with the Alfven and/or slow wave branches. The disadvantage of this technique is that it requires the inversion of a complicated linear operator each time step in the calculation.

The semi-implicit XTOR code [22,26] goes partway towards implementing the full ideal MHD operator as given in Eq. (20b). Their method approximates the full ideal MHD operator in Eq. (20b) as the full ideal MHD operator based on the equilibrium fields plus a small coefficient multiplying the Laplacian as follows:

$$\mathbf{G}\{\dot{\mathbf{V}}\} \to \mathbf{G}_0\{\dot{\mathbf{V}}\} + c\nabla^2\{\dot{\mathbf{V}}\}. \tag{21}$$

Thus, the constant c in Eq. (21) could be very small compared to that used in [20] since it is needed only for the small departure of the computed nonlinear solutions from their linear eigenmodes. This was implemented in toroidal geometry using a spectral representation in both the poloidal and toroidal angles. The stabilizing implicit operator $\mathbf{G}$ was included in both steps of a predictor–corrector scheme in [22] and in only the second step of a modified predictor–corrector scheme in [26]. Resistive terms are included in an implicit resistive advance for the magnetic field in a separate step after the corrector step.

The NIMROD code [27,28] uses basically the same implicit operator as given in Eq. (21), but combines this with an explicit leap-frog scheme. However, they also include the symmetric part of the deviation of the solution from equilibrium in the operator $\mathbf{G}_0$ in Eq. (21), and the constant c is computed to be the maximum difference between the actual and equilibrium fast wave speed. This has been implemented using high-order finite elements in the poloidal plane and a spectral representation in the toroidal angle.

The M3D-C^1 code line has implemented a similar algorithm for nonlinear calculations in 2D [29,30] and linear calculations in 3D [31,32] in which the full ideal MHD operator in Eq. (20b) has been implemented. In [30] they describe implementing a general method which can be invoked as either the semi-implicit method using the full implicit operator (which they call the Caramana method [24]) or as the split θ-implicit method which one obtains if Eqs. (19b) and (19c)

are substituted into Eq. (19a) and all terms are retained. Consider now the general algorithm that has three implicit parameters: θ, α, ϕ, and offset time levels.

$$(\rho\mathbf{I} - \theta^2\delta t^2\mathbf{G})\mathbf{V}^{n+1} = (\rho\mathbf{I} - \alpha\delta t^2\mathbf{G})\mathbf{V}^n + \delta t\left[-\nabla p + \frac{1}{\mu_0}(\nabla\times\mathbf{B})\times\mathbf{B}\right]^m - \rho\delta t\left[(1-2\theta)\mathbf{V}^n\cdot\nabla\mathbf{V}^n + \theta(\mathbf{V}^{n+1}\cdot\nabla\mathbf{V}^n + \mathbf{V}^n\cdot\nabla\mathbf{V}^{n+1})\right] \tag{22a}$$

$$\begin{bmatrix} p \\ \mathbf{B}\end{bmatrix}^{m+1} = \begin{bmatrix} p \\ \mathbf{B}\end{bmatrix}^{m} + \delta t\phi\begin{bmatrix} f(p^{m+1},\mathbf{V}^{n+1}) \\ \mathbf{g}(\mathbf{B}^{m+1},\mathbf{V}^{n+1})\end{bmatrix} + \delta t(1-\phi)\begin{bmatrix} f(p^{m+1},\mathbf{V}^{n}) \\ \mathbf{g}(\mathbf{B}^{m+1},\mathbf{V}^{n})\end{bmatrix}, \tag{22b}$$

Here, $\mathbf{G}$ is the full ideal MHD operator given in Eq. (20b), $\mathbf{I}$ is the identity operator, and f and $\mathbf{g}$ are the functions implied by Eqs. (19b) and (19c). Setting $m = n + 1/2$ corresponds to the leap-frog treatment of the explicit terms. If we linearized about a configuration with $\mathbf{V} = 0$ and consider an eigenmode such that $\mathbf{G}\{\mathbf{V}\} = \lambda_i\mathbf{V}$, defining $D \equiv -\delta t^2\lambda_i$, we find that the amplification factor, r, satisfies the quadratic equation

$$(1+\theta^2 D)(r-1)^2 + D(\theta^2+\phi-\alpha)(r-1) + D = 0. \tag{23}$$

Analysis of the roots of Eq. (23) shows that for the Caramana method, for which $\phi = 1$ and $\alpha = \theta^2$, we have $|r|^2 = 1$ corresponding to linear stability and no-dissipation for $\theta \geqslant 1/2$. Truncation error analysis shows the time discretization error to be second-order in δt for any stable value of θ. This method has the additional feature that the multiplier of the operator $\mathbf{G}$ is the same on both sides of Eq. (22a), so that in steady state, when $\mathbf{V}^{n+1} = \mathbf{V}^n$, the operator will have no effect on the solution.

For the split θ-implicit method, for which $\phi = \theta$ and $\alpha = \theta(\theta-1)$, the amplification factor is less than or equal to 1 (and hence stable) when $\theta \geqslant 1/2$. However in this case $|r|^2 = 1$ only when $\theta = 1/2$ as the method is dissipative for$\theta > 1/2$. It is also second-order accurate only for $\theta = 1/2$. When the resistive terms are treated implicitly in the time advance for $\mathbf{B}$ (but not included in the operator $\mathbf{G}$) it does not affect the numerical stability.

Breslau and Fu [33] have found that the approximate (of order ε) separation of the MHD wave characteristics into different components of the momentum equation in M3D allows them to approximately split the operator in Eq. (20) and to use a different operator in different projections of the momentum equation to obtain stability to both the fast wave and shear Alfven wave for a range of time steps. Thus, for the divergence of the momentum equation, they replace $\mathbf{G}$ with the semi-implicit operator: $(B^2 + \gamma\ p)R^2\nabla\cdot R^{-2}\nabla$, while for the toroidal component of the curl of the momentum equation and for the toroidal component, they replace the operator $\mathbf{G}$ with the semi-implicit operator: $(\mathbf{B}\cdot\nabla)\mathbf{B}\cdot\nabla$. While not providing numerical stability for an arbitrarily large time step, this allowed approximately an order of magnitude increase in time step over that allowed by the CFL condition for the Alfven wave.

3.6. Non-linear implicit methods

The implicit methods discussed so far utilize a linearization either about the initial equilibrium or about the current state in order to construct the implicit operator needed to advance to the next time step. Another class of methods [34,35] use Jacobian-free Newton–Krylov techniques [36] to solve iteratively for the new time values that self-consistently satisfy the nonlinearly implicit equations. The entire system of discretized nonlinear MHD equations is considered as a single system to which the nonlinear Newton–Krylov method is applied. However, it is found that it is much more efficient [34] to break up the linear solves that occur during each Newton step into smaller subsystems and to iterate between these subsystems using predictor corrector techniques to obtain a converged solution.

Let $\mathbf{V}^{\overline{n+1}}$ be the approximate value of the new time velocity $\mathbf{V}^{n+1}$, and define the difference as $\delta\mathbf{V} \equiv \mathbf{V}^{n+1} - \mathbf{V}^{\overline{n+1}}$. Adopting similar notation for the other variables, the residual of the momentum equation at a given Newton iteration is defined as:

$$\mathbf{R}_\mathbf{v} = \rho^{\overline{n+1}}\left(\mathbf{V}^{\overline{n+1}} - \mathbf{V}^n\right) + \theta\delta t\left[\rho^{\overline{n+1}}\mathbf{V}^{\overline{n+1}}\cdot\nabla\mathbf{V}^{\overline{n+1}} + \nabla p^{\overline{n+1}} - \mathbf{J}^{\overline{n+1}}\times\mathbf{B}^{\overline{n+1}}\right] + (1-\theta)\delta t[\rho^n\mathbf{V}^n\cdot\nabla\mathbf{V}^n + \nabla p^n - \mathbf{J}^n\times\mathbf{B}^n]. \tag{24a}$$

Similarly, the residuals for the density, pressure, and magnetic field are given by:

$$R_\rho\left(\rho^{\overline{n+1}}\right) = \left(\rho^{\overline{n+1}} - \rho^n\right) + \theta\delta t\nabla\cdot\left(\rho^{\overline{n+1}}\mathbf{V}^{\overline{n+1}} - D\nabla\rho^{\overline{n+1}}\right) + (1-\theta)\delta t\nabla\cdot(\rho^n\mathbf{V}^n - D\nabla\rho^n), \tag{24b}$$

$$R_p\left(p^{\overline{n+1}}\right) = \left(p^{\overline{n+1}} - p^n\right) + \theta\delta t\left[\mathbf{V}^{\overline{n+1}}\cdot\nabla p^{\overline{n+1}} + \gamma p^{\overline{n+1}}\nabla\cdot\mathbf{V}^{\overline{n+1}}\right] + (1-\theta)\delta t[\mathbf{V}^n\cdot\nabla p^n + \gamma p^n\nabla\cdot\mathbf{V}^n] + \nabla\cdot\mathbf{q}, \tag{24c}$$

$$\mathbf{R}_\mathbf{B}\left(\mathbf{B}^{\overline{n+1}}\right) = \left(\mathbf{B}^{\overline{n+1}} - \mathbf{B}^n\right) + \theta\delta t\left[\nabla\times\left(\mathbf{V}^{\overline{n+1}}\times\mathbf{B}^{\overline{n+1}}\right) - \frac{\eta}{\mu_0}\nabla\times\nabla\times\mathbf{B}^{\overline{n+1}}\right] + (1-\theta)\delta t\left[\nabla\times(\mathbf{V}^n\times\mathbf{B}^n) - \frac{\eta}{\mu_0}\nabla\times\nabla\times\mathbf{B}^n\right]. \tag{24d}$$

At each step in the Newton iteration, the corrections to the density, pressure, magnetic field and velocity are determined as follows:

Step 1: Predictor step for the field quantities at fixed velocity

$$\delta\rho^* = -\left[\frac{\partial R_\rho}{\partial \rho^{\overline{n+1}}}\right]^{-1} \cdot R_\rho, \qquad \delta p^* = -\left[\frac{\partial R_p}{\partial p^{\overline{n+1}}}\right]^{-1} \cdot R_p, \qquad \delta\mathbf{B}^* = -\left[\frac{\partial \mathbf{R_B}}{\partial \mathbf{B}^{\overline{n+1}}}\right]^{-1} \cdot \mathbf{R_B}. \tag{25a}$$

Step 2: Velocity update

$$(\rho\mathbf{I} - \theta^2\delta t^2\mathbf{G})\delta\mathbf{V} = -\mathbf{R}_v + \theta\delta t\begin{bmatrix} -\rho\delta\mathbf{V}\cdot\nabla\mathbf{V} - \rho\mathbf{V}\cdot\nabla\delta\mathbf{V} - \delta\rho^*\mathbf{V}\cdot\nabla\mathbf{V} - \nabla\delta p^* \\ +\frac{1}{\mu_0}(\nabla\times\delta\mathbf{B}^*)\times\mathbf{B} + \frac{1}{\mu_0}(\nabla\times\mathbf{B})\times\delta\mathbf{B}^* \end{bmatrix}. \tag{25b}$$

Step 3: Corrector step for the field quantities

$$\begin{aligned} \delta\rho &= \delta\rho^* - \theta\delta t\nabla\cdot(\rho\delta\mathbf{V}), \\ \delta p &= \delta p^* - \theta\delta t[\delta\mathbf{V}\cdot\nabla p + \gamma p\nabla\cdot\delta\mathbf{V}], \\ \delta\mathbf{B} &= \delta\mathbf{B}^* + \theta\delta t\nabla\times(\delta\mathbf{V}\times\mathbf{B}). \end{aligned} \tag{25c}$$

The operator on the left in Eq. (25b) is the same as that in Eq. (22a). The authors of this method refers to the inclusion of this term as "parabolization" of the equations, and to the technique as a "physics based preconditioner". It is implied that this term is essential to obtain good performance in the iteration. Performing just a single Step 2 (with $\mathbf{V}^{\overline{n+1}} = \mathbf{V}^n$, etc.) and then combining Steps 3 and 1 appears to be equivalent to the method in Eq. (22) with $\alpha = \theta^2$ and $\phi = \theta$ so that this is seen to be a way of generalizing that method to account for the non-linearity in the implicit solve.

This method has been implemented using a multi-grid preconditioner and FGMRES [37] as the Krylov solver for a Cartesian finite volume discretization [34]. A very similar nonlinearly implicit Newton–Krylov method has now been implemented in the XTOR-2F code [35] using the NITSOL package [38]. The primary difference is that the XTOR-2F uses a direct solver for the preconditioner and uses linear finite differences in the radial (equilibrium flux) coordinate and a Fourier representation in the poloidal and toroidal angles.

3.7. Unsplit implicit solves

In the methods described in Sections 3.1–3.6 above, the implicit time advance is split in that the advance for the velocity and the field quantities are done sequentially (although in the method in Section 3.6, these are cycled through iteratively each time step so that the final solution at the end of a time step can be considered unsplit). There are also several algorithms that advance the velocity and field variables on an equal footing in a full unsplit nonlinearly implicit [39–44] or linearly implicit [45–48] solve. The matrices that enter the unsplit solves are known to be poorly conditioned. However these works have shown that unsplit solves are feasible if direct matrix inversion methods or specially preconditioned iterative methods are used. In algorithms in which the angular spatial coordinates are represented as Fourier series and only one coordinate is represented by finite differences, the matrices take on a block tridiagonal form for which a direct solve is particularly efficient [45,46,39].

There have also been efforts to solve the full implicit unsplit system using alternating direction implicit (ADI) methods [49–51]. While stable solutions have been obtained with time steps 10 or more times the CFL limit for a purely explicit method, it has not yet been demonstrated that this is a viable technique for use in a highly anisotropic configuration such as one with realistic geometry as shown in Fig. 1 and with parameters of a magnetic fusion experiment.

A finite volume implicit method is presented in [52] that is based on an approximate Riemann solver for the hyperbolic fluxes [53] and central differencing for the parabolic fluxes. The implicit operator is inverted using an iterative lower upper symmetric Gauss–Seidel technique [54]. It was demonstrated for a problem in model geometry that this technique could produce a CPU savings of a factor of 3 compared to a comparable explicit method.

Several papers have also appeared recently in which a Newton–Krylov solver with an operator-based preconditioner based on directional splitting [55,56] and multi-grid techniques [57] have been applied to the MHD equations in model geometry. While these initial studies look promising, it remains to be seen the applicability of these methods to the calculation of global dynamics of magnetic fusion devices with realistic parameters and geometry.

3.8. Time discretization error

The implicit methods discussed in Sections 3.1–3.6 are of at most 2nd order accurate in time, which means that there is a term in the truncation error proportional to the square of the time step, $(\delta t)^2$. It is natural to ask how this term affects the solution as δt becomes large. We can gain some insight into this question by examining the amplification and phase factors as a function of the linear eigenvalues of the operator $\mathbf{G}$ as given in the dispersion relation Eq. (23). For this analysis, we assume isotropic plane wave solutions so that $\mathbf{G}\{\mathbf{V}\} = -k^2c^2\rho_0\mathbf{V}$, where k and c are the wave number and wave velocity associated with eigenvalue λ of the operator $\mathbf{G}$, and ρ_0 is the plasma density (assumed constant). This implies that the quantity D that appears in Eq. (23) is given by $D = \delta t^2k^2c^2\rho_0$. Letting $r = |r|\exp[i\omega t]$, we plot both the amplification factor $|r|$ and the effective normalized plane wave velocity $u \equiv \omega\delta t/\sqrt{D/\rho_0} \sim \omega/kc$ as a function of the dimensionless quantity $\delta t\ k\ c$. These are

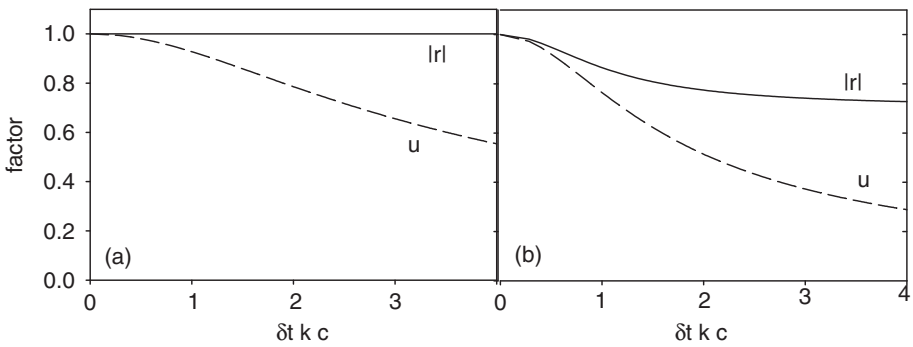

Fig. 2. The amplification factor $|r|$ and the effective normalized wave velocity $u \equiv \omega\delta t/\sqrt{D/\rho_0} \sim \omega/kc$, where k and c are the wave number and wave velocity associated with the operator **G** with eigenvalue $\lambda = -\rho_0 k^2 c^2$: (a) for the Caramana method $(\phi = 1,\ \theta = \frac{1}{2},\ \alpha = \theta^2)$, and (b) for the split θ-implicit method $(\phi = \frac{1}{2},\ \theta = \frac{1}{2},\ \alpha = -\frac{1}{2})$.

shown in Fig. 2a for the Caramana method $(\phi = 1,\ \theta = \frac{1}{2},\ \alpha = \theta^2)$ and in Fig. 2b for the split θ-implicit method $(\phi = \frac{1}{2},\ \theta = \frac{1}{2},\ \alpha = -\frac{1}{2})$.

An intuitive way to interpret Fig. 2 is that if we associate an "effective wavelength" $\Delta x_{eff} \equiv 1/k$ with a perturbation with wavenumber k, then using a time step that exceeds the "effective Courant condition" for that wavelength $\delta t > \Delta x_{eff}/c = 1/kc$ (or $\delta t k\, c > 1$) will lead to errors for that perturbation. In the Caramana method (a), these are strictly errors in the propagation velocity (dispersion), whereas in the θ-implicit method (b) these show up as both errors in the magnitude (dissipation) and in the dispersion.

Some additional insight into the time discretization error of the Caramana method can be obtained by approximating the form of Eq. (22a) linearized about an equilibrium with zero velocity as the partial differential equation

$$\left\{\rho_0 \mathbf{I} - \frac{1}{4}\delta t^2 \mathbf{G}\right\} \frac{\partial^2 \xi}{\partial t^2} = \mathbf{G}\{\xi\}. \tag{26}$$

Here we have introduced the linearized plasma displacement $\xi(\mathbf{x},t)$, related to the velocity by $\mathbf{V} = \partial\,\xi/\partial t$[23], Taylor expanded the velocities $\mathbf{V}^n$ and $\mathbf{V}^{n+1}$ about time point $m = n + 1/2$, and only kept the lowest order terms in the Taylor series involving the operator **G**[58]. It is clear from Eq. (26) that the effect of the implicit time differencing is to introduce an effective "k-dependent density" to the MHD equations that will preferentially slow down the short wavelength disturbances for δt large. If we now let $\partial^2\xi/\ \partial t^2 \to -\omega^2\xi$ and $\mathbf{G}\{\xi\} \to -k^2c^2\rho_0\xi$, we see that the dispersion relation associated with Eq. (26) becomes

$$\frac{\omega}{k} = \frac{c}{\left[1 + \frac{1}{4}\delta t^2 k^2 c^2\right]^{1/2}}. \tag{27}$$

Eq. (27) shows explicitly that the propagation velocity for a disturbance with a given wavenumber k will be reduced as the denominator on the right becomes large. If we again introduce the effective wavelength $\Delta x_{eff} = 1/k$ associated with a perturbation with wavenumber k, we find that the effective Courant number for that wavelength becomes

$$\frac{\delta t}{\Delta x_{eff}}\frac{\omega}{k} = \delta t\ k\frac{\omega}{k} = \frac{\delta t k c}{\left[1 + \frac{1}{4}\delta t^2 k^2 c^2\right]^{1/2}} \tag{28}$$

The quantity on the right is seen to approach a constant as $\delta\ t \to \infty$, so that the effective Courant number associated with a disturbance of a fixed size does not increase without bound as the time step is increased. This property has been used to show that when implicit differencing is applied to the Navier–Stokes equations, there is a close relation to the Navier–Stokes α (NS-α) equations [59] that filter the fluid motion that occurs below some length scale, $\alpha \sim \delta t/c$ [60].

We conclude that if the accurate dynamics of structures of size $\Delta\ x_{eff}$ that propagate with speed c are required, then the time step of the implicit method should be limited to $\Delta t < \Delta\ x_{eff}/c$ for accuracy considerations. However, if the problem of interest involves slow dynamics such as the resistive timescale growth of a global structure such as a magnetic island, then the inertial terms in the momentum equation are negligible and so the wave dispersion introduced by the implicit time advance should not lead to inaccuracies as long as the mode growth is small compared to the timestep, $\delta t\partial/\partial t \leqslant 1$.

4. Spatial representation

It has been recognized since the 1970s that special care must be given to the spatial representation of the magnetic and velocity vector fields in highly magnetized plasma if interest lies in computing unstable motions. Not only must the divergence of the magnetic field be constrained to vanish, but the treatment must be such as to accurately describe a flow field that avoids compressing the strong externally imposed magnetic field to a large degree [61]. In linear MHD, this latter

property has been called the avoidance of spectral pollution [25]. There have been several approaches to satisfying these requirements.

One approach is to construct a representation based on ordering assumptions using the toroidal aspect ratio ε as a small parameter. To lowest order in this parameter, unstable motions of tokamaks can be well described by just two scalar functions: a flux function for the magnetic field and a stream function for the incompressible flow field. This was first introduced in 2D cylindrical geometry [62] and then generalized to 3D [63,64] and extended to higher order in ε and more variables [65–67]. This led to a fully general representation of the velocity and magnetic vector potential fields involving five scalar quantities. If we use a cylindrical (R, ϕ, Z) coordinate system, and denote by $\nabla_\perp$ the gradient in the (R, Z) plane, the vector fields in a tokamak can be represented as [31]:

$$\mathbf{V} = R^2\nabla U \times \nabla\phi + R^2\omega\nabla\phi + R^{-2}\nabla_\perp\chi, \tag{29a}$$

$$\mathbf{A} = R^2\nabla\phi \times \nabla f + \psi\nabla\phi - F_0 \ln R\widehat{Z}. \tag{29b}$$

Here F_0 is a constant proportional to the total current in the toroidal field coils. The particular representation for the vector potential in Eq. (29b) has the associated gauge condition $\nabla_\perp \cdot R^{-2}\mathbf{A} = 0$. This has been found to be convenient [68,31], but is certainly not the only choice possible.

The first two terms in Eq. (29a) do not compress the strong externally imposed toroidal field and will thus be the dominant contribution to the flow field describing a global instability in a tokamak. (The second term in Eq. (29a) has also been taken to be in the direction of the magnetic field, $\mathbf{B} = \nabla \times \mathbf{A}$ [48,68].) Approximate formulations based on an aspect ratio expansion will omit the second and/or third term in Eq. (29a) to obtain a "reduced" set of equations that is capable of describing the dominant plasma motion but is free of this compressible term that leads to the fast wave [67,48]. If this third term is kept, taking appropriate projections of the momentum equation will approximately isolate the fast wave motion to separate equations, which are then solved by implicit techniques, and this term will effectively serve as a small correction to the dominantly compression-free motion [31]. The factor of R^{-2} in the last term in Eq. (29a) is shown to make the first and last terms in that equation orthogonal in the sense that the cross product involving these will vanish when V^2 is integrated over the torus volume (note that in cylindrical geometry, the factors of R^2 or R^{-2} become constants [45,69].) Implicit methods that are based on finite elements that use these and similar representations contain higher order spatial derivatives than occur when using scalar projections of the vector fields and thus benefit from using elements with continuous first derivatives that can represent spatial derivatives up to 4th order when applying the Galerkin method [73,47].

The other technique that has been shown to be effective is to use high-order spatial discretization to represent the scalar projections of the vector fields in a cylindrical or other coordinate system. In addition, it is desirable to separate out equilibrium from non-equilibrium fields, and to use the equilibrium equation to analytically remove the zero order terms. This has been demonstrated using high-order Lagrangian finite elements [28] and high-order spectral elements [40,42,83]. If the magnetic field is advanced rather than the magnetic vector potential, divergence cleaning can be used to enforce the condition $\nabla \cdot \mathbf{B} = 0$[28]. In addition, the form used for the momentum equation can have a large impact on the cumulative error when there is a $\nabla \cdot \mathbf{B}$ error present [70].

A number of published algorithms have used a spectral representation in two of the angle coordinates as a way of accurately computing derivatives of scalar fields [12,15,19,69,20,46,22,39,26]. While this technique has proven effective in representing internal instabilities in mildly shaped tokamaks, it is not clear how effective it will be in representing more shaped, separatrix limited plasmas, where the solution domain is extended to the highly resistive plasma on the open field lines out to the vacuum vessel wall. (However, [71] demonstrates that this is feasible to some extent, at least in 2D). In contrast, recent studies have shown that the use of high-order finite elements in the poloidal plane can handle this geometry to very high accuracy [72,32].

5. The heat-flux term

The thermal conductivity in a high-temperature magnetized plasma is extremely anisotropic due to the fact that charged particles can free-stream parallel to the magnetic field but are confined perpendicular to it. Consider the temperature evolution equation in the presence of anisotropic thermal conduction. Neglecting terms arising from convection and compression, we have

$$\frac{3}{2}n\frac{\partial}{\partial t}T = -\nabla \cdot \mathbf{q} + S, \tag{30a}$$

where the heat flux vector is of the form

$$\mathbf{q} = -n\left[\chi_\parallel \mathbf{bb} + \chi_\perp(\mathbf{I} - \mathbf{bb})\right] \cdot \nabla T. \tag{30b}$$

Here, $\chi_\parallel$ and $\chi_\perp$ are the thermal conductivities parallel and perpendicular to the direction of the magnetic field, $\mathbf{b}$ is a unit vector in the direction of the magnetic field, $\mathbf{I}$ is the identity matrix, and S represents a volumetric source term. Since this is an equation for the temperature that depends only on the temperature, it can normally be solved separately from the other equations in a "time step splitting" fashion.

The concern in solving this equation is that if $\chi_\parallel \gg \chi_\perp$, errors proportional to $\chi_\parallel$ will tend to dominate the solution in the perpendicular direction, making the effective value of $\chi_\perp$ much larger than the specified value. It has been demonstrated that by using high order finite elements, values of $\chi_\parallel$ up to 10^8times larger than $\chi_\perp$ can be used without causing unacceptable pollution in the perpendicular direction [28,73]. Lutjens [26] reports solving anisotropic thermal conduction with a ratio $\chi_\parallel/\chi_\perp \simeq 3 \times 10^4$ using a preconditioned conjugate gradient method in a mixed spectral/finite difference representation. It has also been reported that high order spectral elements yield a given accuracy with less total degrees of freedom than lower-order elements, especially when significant grid misalignment was present [74,42].

Günter, et al. [75,76] demonstrated that even low order finite differences or finite elements can be used to compute highly anisotropic heat conduction accurately if a certain procedure is followed. The prescription is to first calculate temperature gradients at locations staggered from the locations where the temperatures are defined. These gradients are used to calculate parallel heat flux vectors at those same locations. The divergence of the parallel heat flux is then calculated in a conservative manner that maintains the self-adjointness of the operator.

Park, et al. [77,78] introduced an "artificial sound" method to represent the fast thermal equilibration along field lines. Instead of solving an equation like Eq. (30), they solve additional wave equations for the temperature:

$$\frac{\partial T}{\partial t} = \frac{s}{\rho}\mathbf{B}\cdot\nabla u, \tag{31a}$$

$$\frac{\partial u}{\partial t} = s\mathbf{B}\cdot\nabla T - \nu\nabla^2 u. \tag{31b}$$

The wave speed, a constant s times $B/\rho^{1/2}$ (the Alfvén speed), represents the free streaming velocity of electrons with a dissipation ν. The thermal energy inside a flux tube is conserved with this technique, and the asymptotic state satisfies $\mathbf{B}\cdot\nabla T = 0$. An explicit difference method can be used to advance Eq. (31) and the temperature will equilibrate much faster than it would if solving Eq. (30) with an explicit method. There is a close connection between this technique and that of dynamic relaxation [2].

6. Two-fluid terms

The basic techniques described here have been extended to the two-fluid description of plasma [79–82,30,83,35]. When applying the method of differential approximation, the stabilizing operator that appears in the momentum equation is the same as that used for MHD [30,83,35]. The implicit treatment of the $\mathbf{J}\times\mathbf{B}$ term that now appears in the time evolution equation for the magnetic field is handled by some much the same way as the $\mathbf{V}\cdot\nabla\mathbf{V}$ term is treated in the momentum equation in Eq. (22a). Thus, in a split leap-frog implicit time advance where the velocity is defined at integer time levels and the magnetic field and pressure are defined at half time levels, the magnetic field time advance can be written as

$$\dot{\mathbf{B}} = \nabla\times\left[\bar{\eta}\left(\mathbf{J}^{n+1/2} + \theta\delta t\dot{\mathbf{J}}\right) - \mathbf{V}^{n+1}\times\left(\mathbf{B}^{n+1/2} + \theta\delta t\dot{\mathbf{B}}\right) + \frac{1}{ne}\left(\mathbf{J}^{n+1/2} + \theta\delta t\dot{\mathbf{J}}\right)\times\left(\mathbf{B}^{n+1/2} + \theta\delta t\dot{\mathbf{B}}\right) - \frac{1}{ne}\nabla\bar{p}_e^{n+1}\right]. \tag{32}$$

In Eq. (32), $\dot{\mathbf{B}} \equiv (\mathbf{B}^{n+3/2} - \mathbf{B}^{n+1/2})/\delta t$, $\dot{\mathbf{J}} \equiv \nabla\times\dot{\mathbf{B}}$, and a bar over a quantity means evaluating the quantity centered in time. Time centering corresponds to choosing the implicit parameter $\theta = 1/2$. A linearly implicit implementation of Eq. (32) will ignore the term proportional to δt^2 [81,30], whereas a nonlinearly implicit implementation will include this with a Newton iteration [83].

The question arises if there is an effective semi-implicit operator for use in the two-fluid magnetic field advance Eq. (32), either to improve the conditioning of the matrix in a semi-implicit time advance or as a "physics based" preconditioner in a nonlinear implicit advance. Harned and Mikic [79] proposed the following semi-implicit modification of the left side of Eq. (32):

$$\begin{aligned}(\mathbf{I} - \mathbf{G})\dot{\mathbf{B}} &= \cdots \\ \mathbf{G} &= \frac{-\theta^2\delta t^2}{(ne\mu_0)^2}(\mathbf{B_0}\cdot\nabla)^2\nabla^2\end{aligned} \tag{33}$$

They report favorable results with this semi-implicit operator for $\theta \geqslant 1/2$ and using for $\mathbf{B_0}$ a large externally imposed field and implementing either using leap-frog centering with the velocity, or using a separate predictor–corrector step for the magnetic field advance. Their application was a 2D helical symmetry calculation where spectral methods were used in the helical coordinate and finite differences were used in the radial coordinate.

Techniques for evaluating the operator in Eq. (33) and using it as a preconditioner for a nonlinear Newton–Krylov solve in 2D reduced 2F MHD are given in [84]. However, a more general analysis of this operator included in a split linearly implicit time advance, such as in Eq. (22) with $m = n + 1/2$, and making some reasonable assumptions regarding the time levels that different quantities are evaluated at shows the presence of a numerical instability in the general case, even if the equivalent of the magnetic field advance, Eq. (22b) is replaced with a predictor–corrector step [83].

Table 1
Summary of 3D MHD codes referenced in text.

Reference	Name	Geometry	Discretization	Time advance	Div B constraint	Vector fields
[50]	IMP	Curvilinear	FD (3)	ADI-Newton	Vector potential	Coordinate projections
[12]	CTD	Cylindrical	FD (1), SP (2)	Semi-implicit	Vector potential	Cylindrical components
[15]		Cartesian	FD (1), SP (2)	Semi-implicit	Vector potential	Cartesian components
[19]		Cartesian/ cylindrical	FD (1), SP (2)	Semi-implicit	Vector potential	Cartesian/cylindrical components
[20]	DEBS	Cylindrical	FD (1), SP (2)	Semi-implicit	Vector potential	Cylindrical components
[46]	FAR	Torus	FD (1), SP (2)	Unsplit, direct solve	Vector potential	Potentials for velocity
[22]		Cylinder	FD (1), SP (2)	Semi-implicit		Cylindrical components
[39]		Torus	FD (1), SP (2)	Unsplit non-linear implicit,	Enforced using B_R	Co and contra
[26]	XTOR	Torus	FD (1), SP (2)	Semi-implicit		Co and contra
[14]	M3D	Toroidal	FE (2),FD (1)	Partially-implicit	Vector potential	Stream ftn./potential
[31]	M3D-C^1	Toroidal	C^1 FE (3)	Split linearly implicit	Vector potential	Stream ftn./potential
[83]	NIMROD	Toroidal	FE (2), SP (1)	Split linearly implicit	Divergence cleaning	Toroidal components
[34]	PIXIE3D	Cartesian	Finite volume	Preconditioned Newton–Krylov	Solenoidal differencing	Cartesian components
[48]	JOREK	Toroidal	Bezier FE (2), SP (1)	Unsplit linearly implicit	Vector potential	Reduced MHD
[41]	BOUT++	Toroidal field align.	Finite difference	Unsplit Newton Krylov (CVODE)	Vector potential	Reduced MHD
[35]	XTOR-2F	Torus	FD (1), SP (2)	Preconditioned Newton–Krylov		Co and contra
[42]	HiFi	Flexible (Cartesian)	Spectral FE	Unsplit Newton–Krylov	Vector potential	Flexible (Cartesian)

A semi-implicit operator of the form of that in Eq. (33) has been successfully implemented as part of an iterative semi-implicit method using a spectral representation of reduced MHD in2D [85]. In [87] they describe a semi-implicit operator based on Eq. (33) implemented in a third-order Runge–Kutta time advance using a spectral method in 3D. In [86] they describe a local specially preconditioned Jacobi-like iteration based on this operator that they demonstrate is effective when used in a multigrid scheme with Cartesian coordinates in 2D.

7. Summary and discussion

Returning to Fig. 1, it is interesting to review what groups have actually attempted to simulate this configuration. Most of the papers cited here have utilized simulation domains that have made some approximations to this geometry. In Table 1 we list the published codes which solve the 3D MHD equations. Papers using the codes CTD (in 2D) [71], M3D [88,89], M3D-C^1[32], NIMROD[72], and JOREK[Huysmans] have reported on calculations that extend outside the separatrix surface to the vacuum vessel, and M3D [89] has included resistivity in the vacuum vessel and thereby extended the solution domain to infinity.

A largely unanswered question has to do with what is the relative advantage of using a nonlinear implicit method [34,41], [42] over one that is linearized about each timestep (which we call here linearly implicit) [83,48]. It is possible that this is problem dependent. In [35], one such comparison is made for the XTOR code and it is stated that the Newton–Krylov non-linearly implicit method is about a factor of 3 more costly than the linearly implicit method for the same accuracy for the resistive MHD case. However, this is likely not a general result.

Another comparison of interest is that between split and unsplit linearly implicit methods, and similarly between un-preconditioned and preconditioned nonlinear implicit methods. One such comparison is made in [30] where it was found that by most measures, the split and unsplit linearly implicit methods had very similar accuracy for the same time step, but that the matrices in the unsplit case were rank 8 N as opposed to two rank 3 N and two rank N matrices in the split linearly implicit case, and thus considerable more effort was required for direct inversion. However, it was found that in one case a non-linear instability occurred in the split case when the transport coefficients were strong functions of the changing temperature, but that a single predictor–corrector iteration corrected this and allowed the split linearly implicit timestep to increase by several orders of magnitude and remain stable. For the Newton–Krylov nonlinear implicit methods, several authors have indicated that including the same operator preconditioner used in the split linearly implicit methods, Eq. (20b), led to greatly improved performance in the iterative solves [34,35].

A great amount of progress has been made since the first papers appeared in which any implicit algorithms for the MHD equations in magnetized plasma were mentioned. Further progress will result from finding the preferred combination of implicit algorithm, spatial representation, and solver methodology, and adapting these techniques to perform efficiently on today's massively parallel computers. This is an area where close collaboration between theoretical and computational physicists, applied mathematicians, and computer scientists will bring great benefits.

Acknowledgments

The author has benefited from discussions, additions, and corrections suggested by J. Breslau, N. Ferraro, A. Glasser, S. Kruger, V. Lukin, D. Schnack, and particularly C. Sovinec. This work was supported by U.S. DoE contract DE-AC02-76CH03073.

Appendix A. Implicit hyperbolic algorithms and relation to Schur complement

First consider the simple wave equation in 1D with constant propagation velocity c:

$$\frac{\partial V}{\partial t} = c\frac{\partial p}{\partial x}, \quad \frac{\partial p}{\partial t} = c\frac{\partial V}{\partial x}. \tag{A-1a}$$

The two equations in Eq. (A-1a) could also be written as a single wave equation for either p or V, *i.e.*

$$\frac{\partial^2 V}{\partial t^2} = c^2\frac{\partial^2 V}{\partial x^2} \tag{A-1b}$$

or

$$\frac{\partial^2 p}{\partial t^2} = c^2\frac{\partial^2 p}{\partial x^2}. \tag{A-1c}$$

Introduce $s \equiv c\delta t/\delta x$, where δt and δx are the time and space increments. A centered in space, backward in time, implicit finite difference method for Eq. (A-1a) corresponds to:

$$V_j^{n+1} = V_j^n + s\left[p_{j+1/2}^{n+1} - p_{j-1/2}^{n+1}\right] \tag{A-2a}$$

$$p_{j+1/2}^{n+1} = p_{j+1/2}^n + s\left[V_{j+1}^{n+1} - V_j^{n+1}\right] \tag{A-2b}$$

A centered in space, backward in time, implicit finite difference method for Eq. (A-1a) is likewise given by

$$V_j^{n+1} - 2V_j^n + V_j^{n-1} = s^2\left[V_{j+1}^{n+1} - 2V_j^{n+1} + V_{j-1}^{n+1}\right]. \tag{A-2c}$$

Note that we can add Eq. (A-2a), with $n \to n-1$, to Eq. (A-2c), and move the advanced time value to the left side of the equation to obtain

$$V_j^{n+1} - s^2\left[V_{j+1}^{n+1} - 2V_j^{n+1} + V_{j-1}^{n+1}\right] = V_j^n + s\left[p_{j+1/2}^n - p_{j-1/2}^n\right] \tag{A-2d}$$

Eq. (A-2d) is also obtained if we use Eq. (A-2b) to algebraically eliminate both $p_{j+1/2}^{n+1}$ and $p_{j-1/2}^{n+1}$ from Eq. (A-2a). This can be solved either iteratively or directly (tridiagonal in 1D) for the new time velocity V_j^{n+1}, which is then, in turn, used in Eq. (A-2b) to solve for the new time pressure $p_{j+1/2}^{n+1}$.

In this 1D simple example where the pressure and velocity appear symmetrically, we could equally as well have used Eq. (A-2a) to eliminate the new time velocity from Eq. (A-2b), and solved an equation identical in form to Eq. (A-2d) to first solve for the new time pressure, and then used this in Eq. (A-2a) to solve for the new time velocity.

Alternatively, as another way of obtaining this same result, we could start with Eqs. (A-2a) and (A-2b) in matrix form:

$$\left[\begin{array}{c|c} \mathbf{A} & \mathbf{B} \\ \hline \mathbf{C} & \mathbf{D} \end{array}\right] \bullet \begin{bmatrix} \mathbf{V} \\ \mathbf{P} \end{bmatrix}^{n+1} = \begin{bmatrix} \mathbf{V} \\ \mathbf{P} \end{bmatrix}^n \tag{A-3}$$

Here **A** and **D** are identity matrices, and **B** and **C** are lower and upper triangular matrices of the form (ignoring boundary conditions):

$$\mathbf{B} = \begin{bmatrix} \cdots & & & & \\ s & -s & & & \\ & s & -s & & \\ & & s & -s & \\ & & & s & \cdots \end{bmatrix}, \quad \mathbf{C} = -\mathbf{B}^T = \begin{bmatrix} \cdots & & & & \\ & s & -s & & \\ & & s & -s & \\ & & & s & -s \\ & & & & \cdots \end{bmatrix}, \quad \mathbf{V} = \begin{bmatrix} \cdots \\ V_{j-1} \\ V_j \\ V_{j+1} \\ \cdots \end{bmatrix}, \quad \mathbf{P} = \begin{bmatrix} \cdots \\ V_{j-1/2} \\ V_{j+1/2} \\ V_{j+3/2} \\ \cdots \end{bmatrix}.$$

Eq. (A-2d) can also be written in matrix form as

$$\mathbf{A}'\mathbf{V}^{n+1} = \mathbf{V}'^n. \tag{A-4}$$

Here the matrix $\mathbf{A}'$ and the vector $\mathbf{V}'^n$ are given by

$$\mathbf{A}' = \begin{bmatrix} \cdots & & & & \\ -s^2 & 1+2s^2 & -s^2 & & \\ & -s^2 & 1+2s^2 & -s^2 & \\ & & -s^2 & 1+2s^2 & -s^2 \\ & & & & \cdots \end{bmatrix}, \quad \mathbf{V}'^n = \begin{bmatrix} \cdots \\ V_{j-1} + s(p_{j-1/2} - p_{j-3/2}) \\ V_j + s(p_{j+1/2} - p_{j-1/2}) \\ V_j + s(p_{j+3/2} - p_{j+1/2}) \\ \cdots \end{bmatrix}^n.$$

This is seen to be simply the Schur Complement of the matrix in Eq. 33, i.e. $\mathbf{A}' = \mathbf{A} - \mathbf{B}\mathbf{D}^{-1}\mathbf{C}$, $\mathbf{V}'^n = \mathbf{V}^n - \mathbf{B}\mathbf{D}^{-1}\mathbf{P}^n$ The matrix in Eq. (A-4) is seen to be half the rank of that in Eq. 33, and is diagonally dominant and symmetric. Once the new time velocity is solved for, the pressure is updated from Eq. (A-2b) without need for further matrix inversion.

Appendix B. The MHD equations

In this paper, we are concerned with three fluid models: ideal MHD, resistive MHD, and two-fluid (2F) MHD. A more complete description of these models can be found in [2]. The equations for the three models are given here. The continuity equation for the number density is:

$$\frac{\partial n}{\partial t} + \nabla \cdot (n\mathbf{V}) = 0. \tag{B-1}$$

MHD assumes that there is no net charge density. For a single species of singly charged ions, the electron and ion densities are therefore equal: $n_e = n_i \equiv n$. Assuming the electron mass is much smaller than the ion mass, $m_e \ll M_i$, the momentum equation for the mass averaged velocity takes the form:

$$\begin{aligned} nM_i\left(\frac{\partial \mathbf{V}}{\partial t} + \mathbf{V} \bullet \nabla \mathbf{V}\right) + \nabla p - \mathbf{J} \times \mathbf{B} &= 0 \quad \text{ideal MHD} \\ &= -\nabla \cdot \Pi_i \quad \text{resistive MHD} \\ &= -\nabla \cdot \Pi_{2F} \quad \text{2F MHD.} \end{aligned} \tag{B-2}$$

The magnetic field must be initialized with $\nabla \cdot \mathbf{B} = 0$. It then evolves according to Faraday's law:

$$\frac{\partial \mathbf{B}}{\partial t} = -\nabla \times \mathbf{E}. \tag{B-3}$$

The divergence condition will remain satisfied by Eq. (33). However, it is often enforced by introducing a vector potential $\mathbf{A}$ such that $\mathbf{B} = \nabla \times \mathbf{A}$, and time advancing $\mathbf{A}$ rather than $\mathbf{B}$. In MHD, the electrical current density is defined as [SI units]

$$\mu_0 \mathbf{J} = \nabla \times \mathbf{B}. \tag{B-4}$$

The generalized Ohm's law equation for the electric field is

$$\begin{aligned} \mathbf{E} + \mathbf{V} \times \mathbf{B} &= 0 \quad \text{ideal MHD} \\ &= \eta \mathbf{J} \quad \text{resistive MHD} \\ &= \eta \mathbf{J} + \frac{1}{ne}[\mathbf{J} \times \mathbf{B} - \nabla p_e] \quad \text{2F MHD.} \end{aligned} \tag{B-5}$$

Here, η is the electrical resistivity and e is the electron charge. The internal energy equation is

$$\begin{aligned} \frac{3}{2}\left[\frac{\partial p}{\partial t} + \nabla \cdot (p\mathbf{V})\right] + p\nabla \cdot \mathbf{V} &= 0 \quad \text{ideal MHD} \\ &= -\nabla \cdot \mathbf{q} + \eta J^2 - \Pi_i : \nabla \mathbf{V} \quad \text{resistive MHD.} \end{aligned} \tag{B-6}$$

The pressure is related to the density and the temperature by $p = p_e + p_i = nk_B(T_e + T_i)$. In ideal and resistive MHD it is normally assumed the electron and ion temperatures are equal. The heat flux vector occurring in Eq. (B-6) is normally of the anisotropic form given in Eq. (30b). In 2F MHD, the energy equation is somewhat more complicated and an additional energy equation needs to be added for either the ions or electrons. For this, and the definition and some common approximations to the stress tensor terms occurring in Eqs. (B-2) and (B-6), the reader is referred to [2].

References

[1] J. Wesson, Tokamaks, Oxford University Press, 2004.
[2] S.C. Jardin, Computational Methods in Plasma Physics, Taylor and Francis, Boca Raton, 2010.
[3] A. Bondeson, D.J. Ward, Stabilization of external-modes in tokamaks by resistive walls and plasma rotation, Phys. Rev. Lett. 17 (1994) 2709–2712.
[4] S.P. Smith, S.C. Jardin, J.P. Freidberg, L. Guazzotto, Numerical calculations demonstrating complete stabilization of the ideal magnetohydrodynamic resistive wall mode by longitudinal flow, Phys. Plasmas 16 (2009) 084504.
[5] J.P. Freidberg, Ideal Magnetohydrodynamics, Plenum Press, New York, 1987.

[6] R. Courant, K.O. Friedrichs, H. Lewy, On the partial differential equations of mathematical physics, IBM J. 11 (1967) 215–234.
[7] B. Coppi, J.M. Greene, J.L. Johnson, Resistive instabilities in a diffuse linear pinch, Nucl. Fusion 6 (1966) 101.
[8] A.H. Glasser, J.M. Greene, J.L. Johnson, Resistive instabilities in general toroidal plasma configurations, Phys. Fluids 18 (1975) 875–888.
[9] P.H. Rutherford, Nonlinear growth of tearing mode, Phys. Fluids 16 (1973) 1903–1908.
[10] F.H. Harlow, A.A. Amsden, Numerical calculation of almost incompressible flow, J. Comput. Phys. 3 (1968) 80–93.
[11] S.C. Jardin, J.L. Johnson, J.M. Greene, R.C. Grimm, Dynamical grid method for time-dependent simulations of axisymmetric instabilities in tokamaks, J. Comput. Phys. 29 (1978) 101.
[12] A.Y. Aydemir, D. Barnes, An implicit algorithm for compressible three dimensional magnetohydrodynamic calculations, J. Comput. Phys 59 (1985) 108–119.
[13] A.Y. Aydemir, J.C. Wiley, D.W. Ross, Toroidal studies of sawtooth oscillations in tokamaks, Phys. Fluids B 1 (1989) 774–787.
[14] W. Park, D. Monticello, Sawtooth oscillations in tokamaks, Nucl. Fusion 30 (1990) 2413–2418.
[15] D.S. Harned, W. Kerner, Semi-implicit method for 3-dimensional compressible magnetohydrodynamic simulation, J. Comput. Phys. 60 (1985) 62.
[16] A.J. Robert, The integration of a spectral model of the atmosphere by the implicit method, in: Proc. WMO/IUGG Symp. on Numerical Weather Prediction, Tokyo, Japan Meteorological Agency, 1-3-4, Ote-machi, Chiyoda-ku, Tokyo, 1969, pp. VII-19–VII-24.
[17] A.J. Robert, J. Henderson, C. Turnbull, An implicit time integration scheme for baroclinic models of the atmosphere, Mon. Wea. Rev. 100 (1972) 329–335.
[18] A. Robert, T.L. Yee, H. Ritchie, A semi-Lagrangian and semi-implicit numerical integration scheme for multilevel atmospheric models, Mon. Wea. Rev. 113 (1985) 388–394.
[19] D.S. Harned, D.D. Schnack, Semi-implicit method for long time scale magnetohydrodynamic computations in three dimensions, J. Comput. Phys. 65 (1986) 57.
[20] D.D. Schnack, D.C. Barnes, Z. Mikic, D.S. Harned, E.J. Caramana, Semi-implicit magnetohydrodynamic calculations, J. Comput. Phys. 70 (1987) 3.
[21] R. Lionello, Z. Mikic, J. Linker, Stability of algorithms for waves with large flows, J. Comput. Phys. 152 (1999) 346–358.
[22] K. Lerbinger, J.F. Luciani, A new semi-implicit method for MHD computations, J. Comput. Phys. 97 (1991) 444.
[23] I.B. Bernstein, E.A. Frieman, M.D. Kruskal, R.M. Kulsrud, An energy principle for hydromagnetic stability problems, Proc. R. Soc. Lond. A 244 (1958) 17.
[24] E.J. Caramana, Derivation of implicit difference schemes by the method of differential approximation, J. Comput. Phys. 96 (1991) 484–493.
[25] R. Gruber, J. Rappaz, Finite Element Methods in Linear Ideal Magnetohydrodynamics, Springer, Berlin, 1985.
[26] H. Lutjens, J. Luciani, The XTOR code for nonlinear 3D simulations of MHD instabilities in tokamak plasmas, J. Comput. Phys. 227 (2008) 6944–6966.
[27] A.H. Glasser, C.R. Sovinec, R.A. Nebel, T.A. Gianakon, S.J. Plimpton, M.S. Chu, D.D. Schnack, The NIMROD code: a new approach to numerical plasma physics, Plasma Physics and Controlled Fusion 41 (1999) A747–A755.
[28] C.R. Sovinec, A.H. Glasser, T.A. Gianakon, D.C. Barnes, R.A. Nebel, S.E. Kruger, D.D. Schnack, S.J. Plimpton, A. Tarditi, M.S. Chu, Nonlinear magnetohydrodynamics simulation using high-order finite elements, J. Comput. Phys. 195 (2004) 355.
[29] S.C. Jardin, J. Breslau, N. Ferraro, A high-order implicit finite element method for integrating the two-fluid magnetohydrodynamic equations in two dimensions, J. Comput. Phys. 226 (2007) 2146–2174.
[30] N.M. Ferraro, S.C. Jardin, Calculations of two-fluid magnetohydrodynamic axisymmetric steady-states, J. Comput. Phys. 228 (2009) 7742–7770.
[31] J. Breslau, N. Ferraro, S. Jardin, Some properties of the M3D-C^1 form of the three-dimensional magnetohydrodynamics equations, Phys. Plasma 16 (2009) 092503.
[32] N.M. Ferraro, S.C. Jardin, P. Snyder, Ideal and resistive edge stability calculations with M3D-C^1, Phys. Plasmas 17 (2010) 102508.
[33] J.A. Breslau, G.Y. Fu, Implementation of an implicit shear Alfven operator in the M3D code, Comput. Phys. Comm. 181 (2010) 1661–1670.
[34] L. Chacon, An optimal, parallel, fully implicit Newton–Krylov solver for three-dimensional viscoresistive magnetohydrodynamics, Phys. Plasmas 15 (2008) 056103.
[35] H. Lutjens, J.F. Luciani, XTOR-2F: a fully implicit Newton–Krylov solver applied to nonlinear 3D extended MHD in tokamaks, J. Comput. Phys. 229 (2010) 8130–8143.
[36] D.A. Knoll, D.E. Keyes, Jacobian-free Newton–Kyrlov methods: a survey of approaches and applications, J. Comput. Phys. 193 (2004) 357.
[37] Y. Saad, A flexible inner-outer preconditioned GMRES algorithm, SIAM J. Sci. Comput. 14 (1993) 461–469.
[38] M. Pernice, H.F. Walker, NITSOL: a Newton iterative solver for nonlinear systems, SIAM J. Sci. Comput. 19 (1998) 302–318.
[39] A.M. Popov, V.S. Chan, M.S. Chu, Y.Q. Liu, B.W. Rice, A.D. Turnbull, Nonlinear three-dimensional self-consistent simulations of negative central shear discharges in the DIII-D tokamak, Phys. Plasmas 8 (2001) 3605.
[40] A. Glasser, X.Z. Tang, The SEL macroscopic modeling code, Comp. Phys. Comm. 164 (2004) 237–243.
[41] B.D. Dudson, M.V. Umansky, X.Q. Xu, P.B. Snyder, H.R. Wilson, BOUT++: a framework for parallel plasma fluid simulations, Comp. Phys. Comm. 180 (2009) 1467–1480.
[42] V.S. Lukin, A.H. Glasser, W. Lowrie, E.T. Meier, Overview of HiFi – implicit spectral element code framework for general multi-fluid applications, J. Comput. Phys., submitted for publication.
[43] J.N. Shadid, R.P. Pawlowski, J.W. Banks, L. Chacon, P.T. Lin, R.S. Tuminaro, Towards a scalable fully-implicit fully-coupled resistive MHD formulation with stabilized FE methods, J. Comput. Phys. 229 (2010) 7649–7671.
[44] S. Ovtchinnikov, F. Dobrian, X.C. Cai, D.E. Keyes, Additive Schwarz-based fully coupled implicit methods for resistive Hall magnetohydrodynamic problems, J. Comput. Phys. 225 (2007) 1919–1936.
[45] J. DeLucia, S.C. Jardin, Nonlinear evolution of the resistive interchange mode in the cylindrical spheromak, Phys. Fluids 27 (1984) 1773.
[46] L.A. Charlton, J.A. Holmes, V.E. Lynch, B.A. Carreras, T.C. Hender, Compressible linear and nonlinear resistive MHD calculations in toroidal geometry, J. Comput. Phys. 86 (1990) 270.
[47] O. Czarny, G. Huysmans, Bezier surfaces and finite elements for MHD simulations, J. Comput. Phys. 227 (2008) 7423–7445.
[48] G. Huysmans, S. Pamela, E. van der Plas, P. Ramet, Non-linear MHD simulations of edge localized modes (ELMs), Plasma Phys. Control. Fusion 51 (2009) 124012.
[49] I. Lindemuth, J. Killeen, Alternating direction implicit techniques for two-dimensional magnetohydrodynamic calculations, J. Comput. Phys. 13 (1973) 181–208.
[50] C. Finan, J. Killeen, Solution of the time-dependent 3-dimensional resistive MHD equations, Comput. Phys. Commun. 24 (1981) 441.
[51] J.A. Breslau, S.C. Jardin, A parallel algorithm for global magnetic reconnection studies, Comput. Phys. Commun. 151 (2003) 8–24.
[52] O.S. Jones, U. Shumlak, D.S. Eberhardt, An implicit scheme for nonideal magnetohydrodynamics, J. Comput. Phys. 130 (1997) 231–242.
[53] A. Harten, High-resolution schemes for hyperbolic conservation laws, J. Comput. Phys. 49 (1983) 357.
[54] S. Yoon, A. Jameson, Lower-upper symmetric-gauss-seidel method for the Euler and Navier–Stokes equations, AIAA J. 26 (1988) 1025.
[55] D.R. Reynolds, R. Samtaney, C.S. Woodward, A fully implicit numerical method for single-fluid resistive magnetohydrodynamics, J. Comp. Phys. 219 (2006) 144–162.
[56] D.R. Reynolds, R. Samtaney, C.S. Woodward, Operator-based preconditioning of stiff hyperbolic systems, SIAM J. Sci. Comput. 32 (2010) 150–170.
[57] M.F. Adams, R. Samtaney, A. Brandt, Toward textbook multigrid efficiency for fully implicit resistive magnetohydrodynamics, J. Comput. Phys. 229 (2010) 6208–6219.
[58] R.F. Warming, J. Hyatt, The modified equation approach to the stability and accuracy analysis of finite-difference methods, J. Comput. Phys. 14 (1974) 159–179.
[59] D.D. Holm, Fluctuation effects on 3D Lagrangian mean and Eulerian mean fluid motion, Physica D. 133 (1999) 215–269.
[60] B.A. Wingate, The maximum allowable time step for the shallow water α model and its relation to time-implicit differencing, Mon. Wea. Rev. 132 (2004) 2719–2731.

[61] M.S. Chance, J.M. Greene, R.C. Grimm, J.L. Johnson, Study of MHD spectrum of an elliptic plasma column, Nucl. Fusion 17 (1977) 65.
[62] M.N. Rosenbluth, D.A. Monticello, H.R. Strauss, R.B. White, Numerical studies of nonlinear evolution of kink modes in tokamaks, Phys. Fluids 19 (1976) 1987–1996.
[63] H.R. Strauss, Nonlinear, three-dimensional magnetohydrodynamics of noncircular tokamaks, Phys. Fluids 19 (1976) 134.
[64] H.R. Strauss, Dynamics of high-beta-tokamaks, Phys. Fluids 20 (1977) 1354.
[65] R. Schmalz, Reduced 3-dimensional, non-linear equations for high-beta plasmas including toroidal effects, Phys. Lett. A 82 (1981) 14–17.
[66] H.R. Strauss, Finite-aspect-ratio MHD equations for tokamaks, Nucl. Fusion 23 (1983) 649–655.
[67] R. Izzo, D. Monticello, J. DeLucia, W. Park, C. Ryu, Reduced equations for finite beta tearing modes in tokamaks, Phys. Fluids 28 (1985) 903.
[68] E.K. Maschke, J.M. Tosas, A representation of toroidal MHD in terms of stream functions and potentials, Plasma Phys. Controlled Fusion 31 (1989) 563–586.
[69] L. Garcia, H.R. Hicks, B.A. Carreras, L.A. Charlton, J.A. Holmes, 3D nonlinear MHD calculations using implicit and explicit time integration schemes, J. Comput. Phys. 65 (1986) 253–272.
[70] J. Brackbill, D. Barnes, The effect of nonzero $\nabla\cdot\mathbf{B}$ on the numerical solution of the magnetohydrodynamic equations, J. Comput. Phys. 35 (1980) 426–430.
[71] A. Aydemir, An intrinsic source of radial electric field and edge flows in tokamaks, Nucl. Fusion 49 (2009) 065001.
[72] B.J. Burke, S.E. Kruger, C.C. Hegna, P. Zhu, P.B. Snyder, C.R. Sovinec, E.C. Howell, Edge localized linear ideal magnetohydrodynamic instability studies in an extended-magnetohydrodynamic code, Phys. Plasmas 17 (2010) 032103.
[73] S.C. Jardin, A triangular finite element with first-derivative continuity applied to fusion MHD applications, J. Comput. Phys. 200 (2004) 133–152.
[74] E.T. Meier, V.S. Lukin, U. Shumlak, Spectral element spatial discretization error in solving highly anisotropic heat conduction equation, Comp. Phys. Comm. 181 (2010) 837–841.
[75] S.G. Günter, Q. Yu, J. Krüger, K. Lackner, Modeling of heat transport in magnetized plasmas using non-aligned coordinates, J. Comput. Phys. 209 (2005) 354–370.
[76] S. Günter, Finite element and higher order difference formulations for modeling heat transport in magnetized plasmas, J. Comput. Phys. 226 (2007) 2306–2316.
[77] W. Park, D.A. Monticello, H. Strauss, J. Manickam, 3-Dimensional stellarator equilibrium as an Ohmic steady state, Phys. Fluids 29 (1986) 1171.
[78] W. Park, E. Belova, G.Y. Fu, X.Z. Tang, H.R. Strauss, L.E. Sugiyama, Plasma simulation studies using multilevel physics models, Phys. Plasmas (1999) 61796.
[79] D.S. Harned, Z. Mikic, Accurate semi-implicit treatment of the Hall effect in magnetohydrodynamic computations, J. Comput. Phys. 83 (1989) 1–15.
[80] L.E. Sugiyama, W. Park, A nonlinear two-fluid model for toroidal plasmas, Phys. Plasmas 7 (2000) 4644.
[81] C.R. Sovinec, D.D. Schnack, A.Y. Pankin, D.P. Brennan, H. Tian, D.C. Barnes, S.E. Kruger, E.D. Held, C.C. Kimm, X.S. Li, D.K. Kaushek, S.C. Jardin, Nonlinear extended magnetohydrodynamics simulation using high-order finite elements, J. Phys.: Conf. Ser. (2005) 1625–1634.
[82] D.D. Schnack, D.C. Barnes, C.C. Hegna, E.D. Held, C.C. Kimm, S.E. Kruger, A.Y. Pankin, C.R. Sovinec, Computational modeling of fully ionized plasmas using the fluid approximation, Phys. Plasmas 133 (58103) (2006) 1–21.
[83] C.R. Sovinec, J.R. King, Analysis of a mixed semi-implicit/implicit algorithm for low-frequency two-fluid plasma modeling, J. Comput. Phys. 229 (2010) 5803–5819.
[84] L. Chacon, D. Knoll, A 2D high-β Hall MHD implicit nonlinear solver, J. Comput. Phys. 188 (2003) 573–592.
[85] N.F. Loureiro, G.W. Hammett, An iterative semi-implicit scheme with robust damping, J. Comput. Phys. 227 (2008) 4518–4542.
[86] L. Arnold, J. Dreher, R. Grauer, A semi-implicit Hall-MHD solver using whistler wave preconditioning, Comput. Phys. Comm. 178 (2008) 553–557.
[87] D. Laveder, D. Borgogno, T. Passot, P.L. Sulem, On a semi-implicit scheme for spectral simulations of dispersive magnetohydrodynamics, Comput. Phys. Comm. 180 (2009) 1860–1869.
[88] L.E. Sugiyama, H.R. Strauss, Magnetic X-points, edge localized modes, and stochasticity, Phys. Plasmas 17 (2010) 062505.
[89] H.R. Strauss, R. Paccagnella, J. Breslau, Wall forces produced during ITER disruptions, Phys. Plasmas 17 (2010) 082505.